

NASA  
TP  
1693  
c.1

NASA Technical Paper 1693

Off-Design Correlation  
for Losses Due to Part-Span  
Dampers on Transonic Rotors

William B. Roberts, James E. Crouse,  
and Donald M. Sandercock

JULY 1980



LOAN COPY  
AFWL TECH  
KIRTLAND

0067784



TECH LIBRARY KAFB, NM



NASA Technical Paper 1693

Off-Design Correlation  
for Losses Due to Part-Span  
Dampers on Transonic Rotors

William B. Roberts, James E. Crouse,  
and Donald M. Sandercock  
*Lewis Research Center*  
*Cleveland, Ohio*

**NASA**

National Aeronautics  
and Space Administration

**Scientific and Technical  
Information Branch**

1980

## Summary

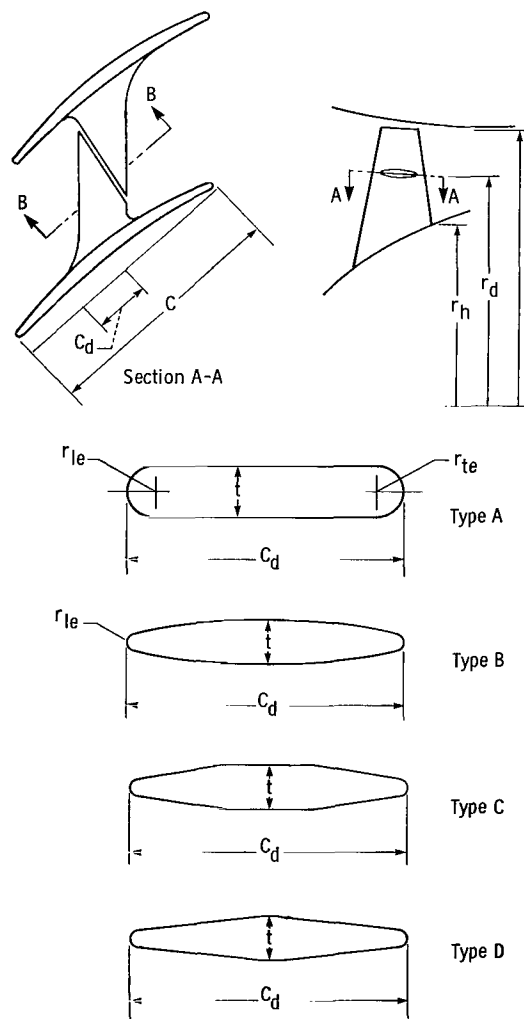
The experimental performance of 10 transonic fan rotors was used to correlate losses caused by midchord part-span dampers during off-design operation between 50 and 100 percent of design speed. The design tip speed for the rotors used varied from 419 to 425 meters per second, and the design pressure ratio varied from 1.6 to 2.0. The loss attributable to the damper and the region influenced along the blade height were correlated with relevant aerodynamic and geometric parameters. The losses at the design point were estimated by using a previously reported correlation as a base. The off-design losses were thus correlated with the variation in blade suction-surface incidence at the damper location. A check with the independent data showed that the prediction of damper losses and region of influence was fair to good for most of the off-design data examined.

## Introduction

Modern fan-jet aircraft engines require high-pressure-ratio, high-bypass-ratio fans of short axial length to minimize both weight and internal and external nacelle drag. This requirement often leads to high-aspect-ratio, transonic blading that necessitates the use of one or more part-span dampers for structural integrity. Figure 1 shows the part-span-damper geometry and typical damper profiles. The use of dampers leads to the need to predict and control their effect on the flow through the rotor. This effect consists of a localized region of additional loss downstream of the rotor, as illustrated in figure 2.

One method of accounting for the damper loss, in design, has been to increase the average overall blade loss to account for the expected decrease in performance. However, this technique does not consider the large temperature and pressure gradients in the region of the damper. Furthermore the blockage and losses associated with the damper can cause flow shifts toward the end-wall regions that may affect performance. Finally the stator blading is often strongly affected, particularly in the region directly behind the damper, by the maldistribution of flow from the rotor. Consequently it would be beneficial to be able to predict the losses due to the

dampers and their regions of influence; then the effects on the localized and overall performance could be calculated and minimized if possible. Reference 1 describes a method of estimating these effects at the design point. The purpose of the present work is to extend the method so that an estimate of damper loss and region influenced can be made for off-design conditions.



Section B-B: Damper profiles used in correlation

Figure 1. - Geometry of part-span dampers.

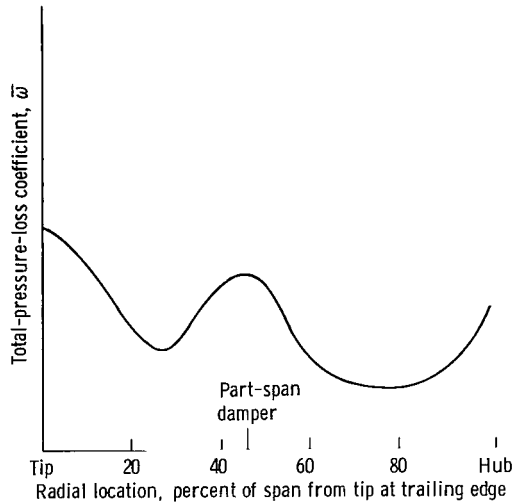


Figure 2. - Radial variation of total-pressure-loss coefficient for rotor with part-span damper.

In reference 2, Esgar and Sandercock show that performance over the blade height can be predicted if the total-pressure-loss distribution is known in the damper region. They took the measured values of energy addition and loss from several transonic rotors with dampers and used these data to calculate the variation of outlet velocity, flow angle, and pressure over the blade span. However, the pressure-loss distribution in the damper region is not generally known before experimental data are obtained. The data from rotors with part-span dampers are examined and correlated herein with selected aerodynamic and geometric parameters to give a method of predicting the localized damper-loss distribution for all normal operating conditions. This can then be added to the estimated loss without a damper to calculate rotor performance.

## Factors Affecting Damper Losses

The losses through transonic rotors caused by part-span dampers can be attributed to several aerodynamic and geometric factors: Mach number, damper angle of attack, maximum damper thickness and aerodynamic chord, damper leading- and trailing-edge thicknesses, blade span in relation to damper geometry, and blade geometry at the damper location.

In reference 3, Benser, et al., describe experiments done on shock-wave visualization by laser hologram in the damper region of a high-tip-speed, transonic fan rotor. Figure 3 shows the interpreted shock system for this rotor at design speed and near-design

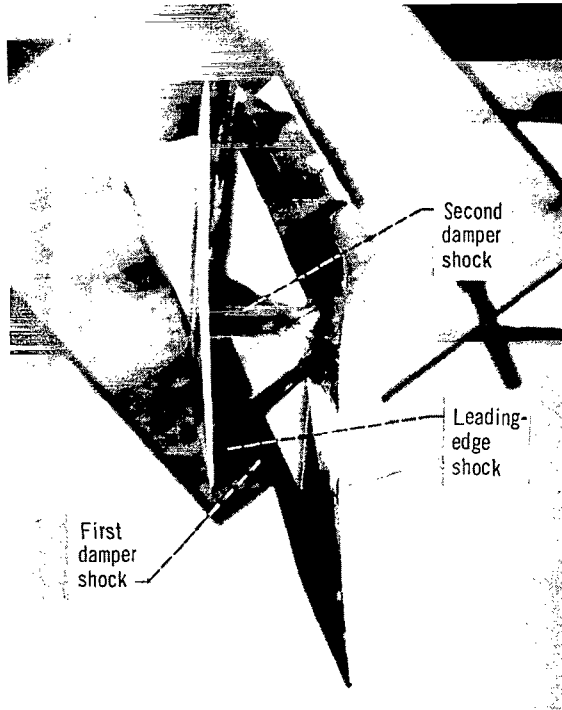
pressure ratio. There is the expected blade leading-edge passage shock, but there are also two shock waves that have been caused by the damper. The first shock starts from the damper leading edge at the blade suction surface and wraps around the damper at an angle to the damper leading edge, and the second comes from the junction of adjacent dampers. Both shocks propagate toward the tip. (It is assumed that a similar propagation of the shocks occurs toward the hub.) Figure 2 illustrates that the loss caused by the damper occurs not in a sharp spike but with a maximum loss at the shroud location and a gradual decrease of loss on either side. The radial propagation of shock waves from the damper, decreasing in intensity with distance, is the probable cause of this difference, as the damper wake could be expected to be relatively small and there would be little mixing measured by a probe placed immediately downstream of the rotor. The strength of the leading-edge damper shock is a function of the Mach number at the damper leading edge, the leading-edge thickness, and the deflection angle (if the damper operates at a nonzero angle of attack). The second shroud shock appears to be caused by the ill fit of the damper bearing surfaces. Therefore the strength of this shock depends on the damper surface Mach number and the radial position of the dampers with respect to each other.

The magnitude of the profile or wake loss is a function of the angle of attack of the damper with respect to the stream surface intersecting the leading edge, the relative thickness of the trailing edge, and (as indicated in ref. 1) the pressure gradients caused by the local blade-to-blade circulation. (This last effect is taken into account by the parameter  $\varphi/\sigma$ .)

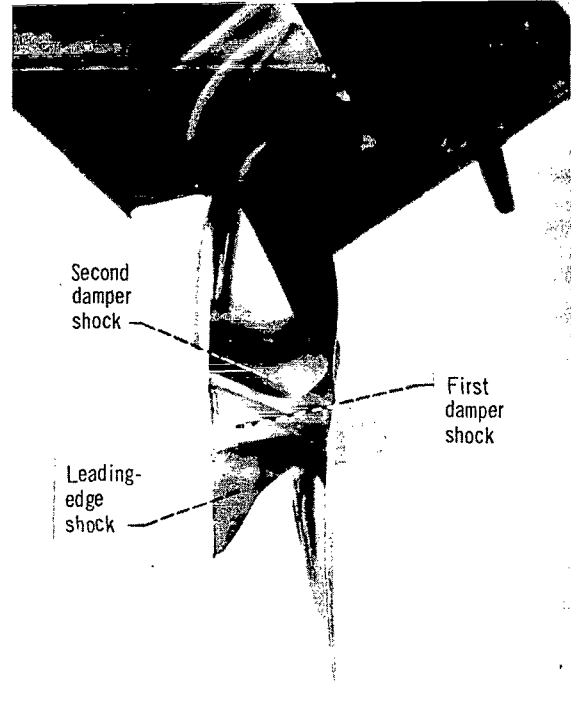
It is clear that the flow in the damper region is highly complex and three dimensional. An analytical or numerical solution of this flow field would require the ability to calculate in three dimensions and would include the effects of viscosity. Presently this is not practical. Therefore an experimental correlation considering the relevant physical parameters must be used to predict losses in the region of the part-span damper.

## Design-Point Loss Correlation

A correlation for the estimation of part-span damper losses at design point is reported in reference 1. This correlation is based on part-span damper losses and on blade-element, design-point aerodynamic and geometric data from 21 transonic, axial-flow research rotors that varied greatly in tip speed and loading. The maximum design-point, total-pressure losses attributable to the damper were



(a) Top view.



(b) Rear view.

Figure 3. - Rotor blade model with shock system at design speed and near-design pressure ratio.

correlated with the following parameters (symbols defined in appendix A):

(1) The shock loss coefficient  $\bar{\omega}_s$  for the blade passage containing the damper, which is the total-pressure-loss coefficient associated with a normal shock of strength  $\bar{M}$  (calculated by the method of ref. 4)

(2) A blade aerodynamic loading parameter, the camber divided by the solidity  $\varphi/\sigma$  at the damper spanwise location

(3) The leading- and trailing-edge damper radii normalized by the mean span and damper chord, respectively,  $r_{le}/h$  and  $r_{te}/c_d$

The tightest data correlation was obtained from the combination of parameters given by

$$\bar{\omega}_{psd,m} = 500 \left( \frac{r_{le}}{h} \right) \bar{\omega}_s + 8 \left( \frac{r_{te}}{c_d} \right) \left( 0.001 + \frac{\varphi}{\sigma} \right) \quad (1)$$

where this relation applies to values of  $r_{le}$  and  $r_{te}$  greater than zero (i.e., if  $r_{le}$  and  $r_{te}$  approach zero,  $\bar{\omega}_{psd,m}$  approaches zero, which is physically

unrealistic). This equation has been changed from that presented in reference 1 by the addition of the constant 0.001 to the term  $\varphi/\sigma$ , which makes the form of the correlation more physically realistic.

Examining the data from the research rotors revealed that the spanwise region influenced by the damper extended over 10 to 15 times the damper maximum thickness, with the damper located near the midpoint of this region. For this correlation a value of 12.5 times the normalized damper thickness was chosen to estimate the spanwise region of influence:

$$\frac{x}{h} = 12.5 \left( \frac{t}{h} \right) \quad (2)$$

The variation of loss in the damper region of influence can be approximated by a modified normal distribution given by the equation

$$\bar{\omega}_{dr} + (\bar{\omega}_{dr,m} - \bar{\omega}_o) \left[ e^{-2(2d/x)^2} - e^{-2(x/2d)^{100}} \right] + \bar{\omega}_o \quad (3)$$



# Off-Design Correlation for Losses due to Part-Span Dampers

## Data Sources, Interpretation, and Accuracy

The large body of experimental data available at the NASA Lewis Research Center was used to correlate off-design, part-span-damper losses. The data from 10 NASA research rotors representing different performance levels were selected as the basis of the correlation. All these rotors used the NASA type B damper (fig. 1) as the type A caused very high losses. The design information for these rotors is given in references 5 to 13, with pertinent information summarized in table I.

Data were sought from NASA-sponsored industrial research for fan rotors with dampers to use as an independent check on the correlation. A search revealed three rotors with some loss definition in the damper region considered herein. One was the first-stage rotor used in the holographic studies mentioned earlier and designed and tested by AiResearch (ref. 14), the second was a single-stage General Electric research fan (ref. 15), and the third was the first-stage rotor from a Pratt & Whitney two-stage, transonic fan (ref. 16). The shapes of the dampers from these three rotors (types D, B, and C, respectively) are shown in figure 1. Pertinent rotor and damper data are given in table I.

The damper loss region was well defined in the NASA tests by five data points taken in the immediate vicinity of the damper, approximately one-half of a chord length downstream. Figure 4 shows a typical radial variation of total-pressure-loss coefficient for a NASA research rotor and demonstrates how the maximum damper loss coefficient  $\bar{\omega}_{psd,m}$  and region of influence were estimated by fairing the radial distribution of the loss coefficient across the damper region as if the damper were not present. It can be seen that the lack of a data point in the region from 60 to 80 percent of span could introduce some error into the estimate of damper maximum loss and region of influence. If at 80 percent of span the loss coefficient were near the design value ( $\sim 0.055$ ), the estimate of maximum damper loss coefficient would be in error by  $\sim 0.01$ . This is typical of most of the data; that is, the estimates of maximum loss coefficient due to the damper were accurate to approximately  $\pm 0.01$ . Likewise the closest that the damper region of influence can be determined is  $\pm 5$  percent of span (i.e.,  $x/h$  to  $\pm 0.05$ ).

For the previously reported design correlations (ref. 1) it was possible to estimate the part-span-

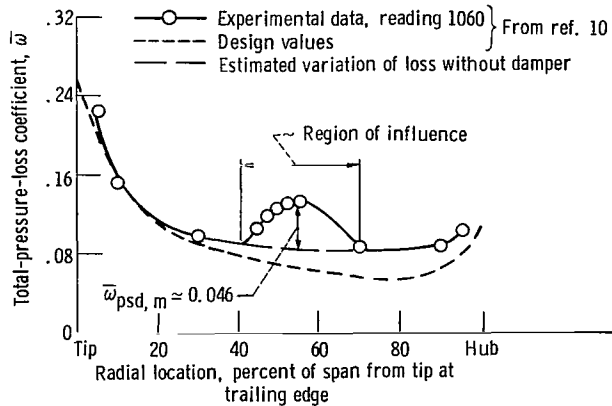


Figure 4. - Radial variation of total-pressure-loss coefficient for NASA rotor 16 at design speed and maximum efficiency.

damper loss by using the data outside the region influenced along with the radial variation of design values. For the off-design case the estimated variation of loss outside the part-span-damper region of influence is much more dependent on the experimental data. To determine the reliability of this technique for off-design use, the radial loss variations of two sets of rotors, similar except for damper size, were compared for various operating conditions. Figure 5 shows the radial loss distributions for NASA rotor 3 (ref. 17) and rotor 3, mod-1 (ref. 18) at 100 and 70 percent of design speed. Three data points on each speed line are plotted for both rotors: near choke, midrange, and near stall. For all conditions the loss variation outside the region influenced by the damper shows the same trends and very nearly the same level, irrespective of damper size. Figure 6 gives the radial loss variation for rotor 1 of the NASA two-stage fan for two speeds at maximum efficiency (refs. 19 to 21). (Rotor 1 was tested with large and small dampers and also without dampers in a low-aspect-ratio configuration.) Again the variation and level of loss are similar, although for the "no damper" rotor the aspect ratio was lower than for the large or small damper blading. These figures indicate that for normal operation the loss variation outside the damper region is not changed significantly by the presence of the damper and that the level of loss is similar. Therefore it should be possible to deduce the approximate radial variation of loss across the blade height in the absence of a damper by using the method illustrated in figure 4. This then was the procedure used to estimate the maximum loss due to the part-span dampers  $\bar{\omega}_{psd,m}$  and the radial extent of influence  $x/h$  for the rotors used in the correlation.

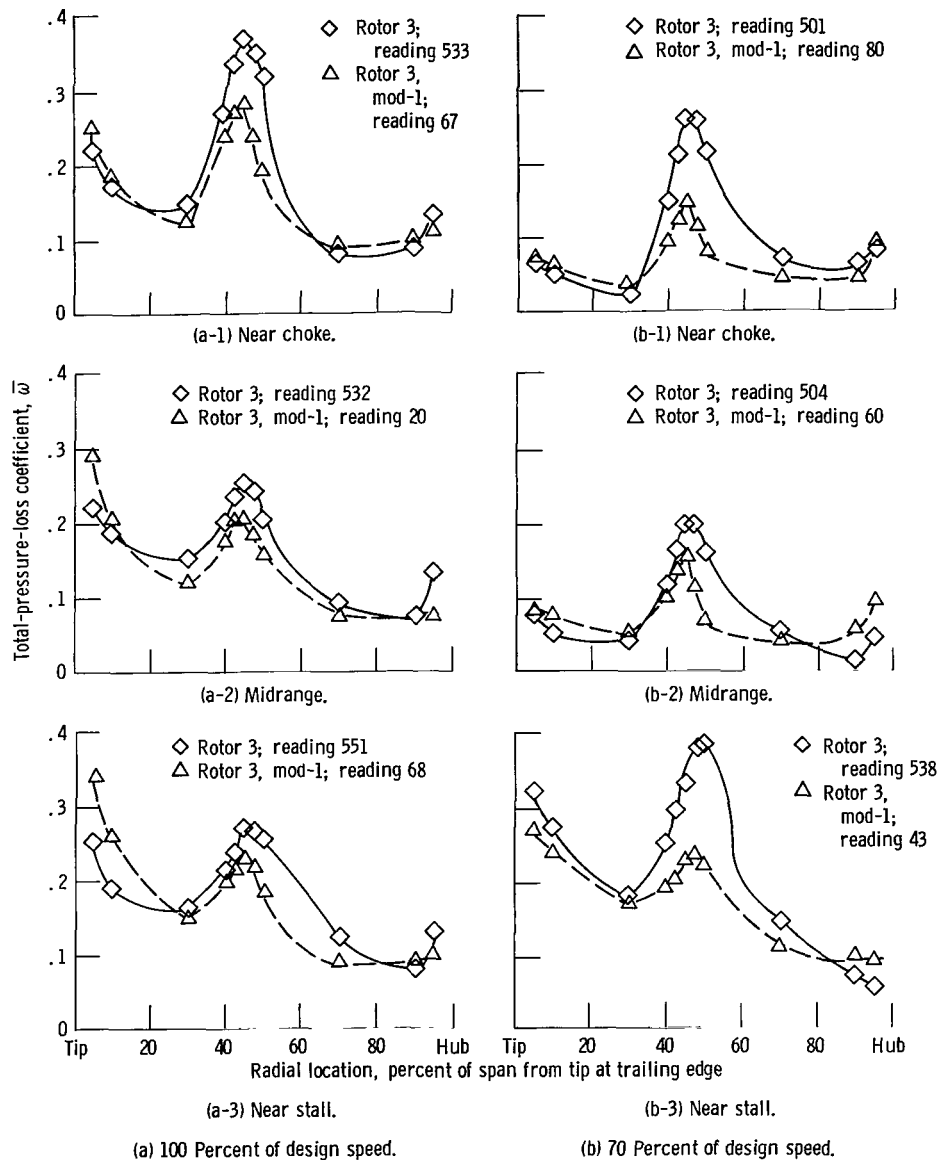


Figure 5. - Radial loss distributions for NASA rotor 3 (large dampers) and NASA rotor 3, mod-1 (small dampers) for various operating conditions.

### Flow-Angle Considerations

If the flow through a rotor in the damper region is modeled as a wing-body combination, the most important single geometric factor affecting off-design performance is the angle of attack of the flow with respect to the damper. This is of course a simplistic assumption, as the flow through a rotor is not axisymmetric but three dimensional. Even so, a mean damper angle of attack would be an important performance parameter. If this were available, we

could postulate off-design loss similar to that of the classical, single-airfoil drag coefficient relation

$$C_D \sim \alpha^2 + C_{D,o}$$

The equivalent expression for damper loss is

$$\bar{\omega}_{psd,m} \sim \alpha^2 + \bar{\omega}_{psd,m}^*$$

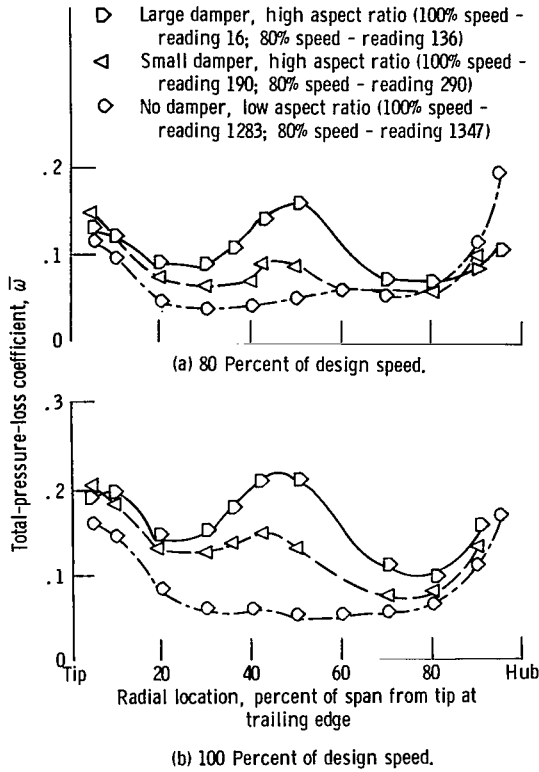


Figure 6. - Radial loss distribution for rotor 1 of NASA two-stage fan with large, small, and no part-span dampers operating near maximum efficiency at 100 and 80 percent of design speed.

where  $\bar{\omega}_{psd,m}^*$  is the minimum and/or reference value. However, the available data have been taken and reduced in such a way that a damper angle of attack is not available. Therefore a substitute must be found that indirectly relates to it. Examining the rotor data shows that at any given rotational speed, damper loss and region of influence go through a minimum as the rotor is throttled from choke to stall. This can be seen in figure 7, where this variation is plotted as a function of equivalent weight flow for NASA rotor 18 (ref. 11).

This figure suggests a relation similar to those just described if damper angle of attack varies directly with weight flow. This should be true for any fixed speed for, as the throttle is closed, the blade incidence increases and thus loads up the rotor and causes some radial shift of streamlines. So equivalent weight flow might be used as a correlation parameter. However, a more direct geometric indicator of blade-section loading at supersonic Mach numbers, and therefore damper performance, would be blade incidence and particularly blade suction-surface incidence  $i_{ss}$  at the damper location.

Figure 8 shows the damper performance of four rotors plotted as a function of blade suction-surface incidence at the damper location for 100 percent of design speed. (Fig. 8 shows blade suction-surface incidences computed from continuity streamlines and therefore their magnitudes may differ somewhat from those computed from design streamlines, as tabulated in most NASA reports, if there is a significant difference in meridional flow angle.) A parabolic relation is evident. Since blade suction-surface incidence is a readily computed geometric parameter, it was used to indirectly correlate damper performance.

### Reference Values

Figure 8 shows large differences in damper performance for different rotors. However, if all damper performance variation with blade suction-surface incidence at the damper location was made relative to a minimum or reference value, there could be some basis of correlation. This was done for five of the rotors from table I (rotors 8, 11, 14, 18, and 21) that had a wide range of loading. A composite plot of these rotor data, reduced relative to the reference, is given in figure 9, where

$$\Delta i_{ss} = i_{ss} - i_{ss}^* \quad (4)$$

$$\Delta \bar{\omega}_{psd,m} = \bar{\omega}_{psd,m} - \bar{\omega}_{psd,m}^* \quad (5)$$

and

$$\Delta(x/h) = \left(\frac{x}{h}\right) - \left(\frac{x}{h}\right)^* \quad (6)$$

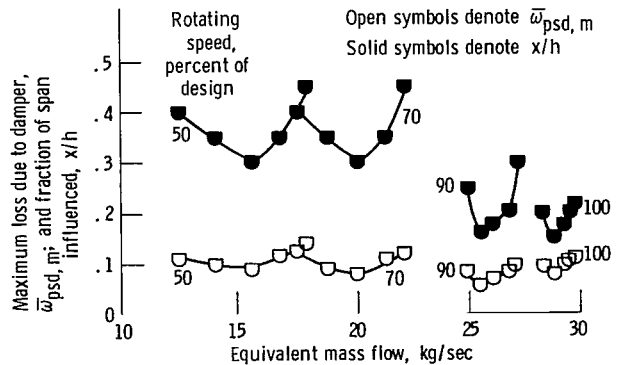


Figure 7. - Performance of part-span damper as function of equivalent mass flow for NASA rotor 18.

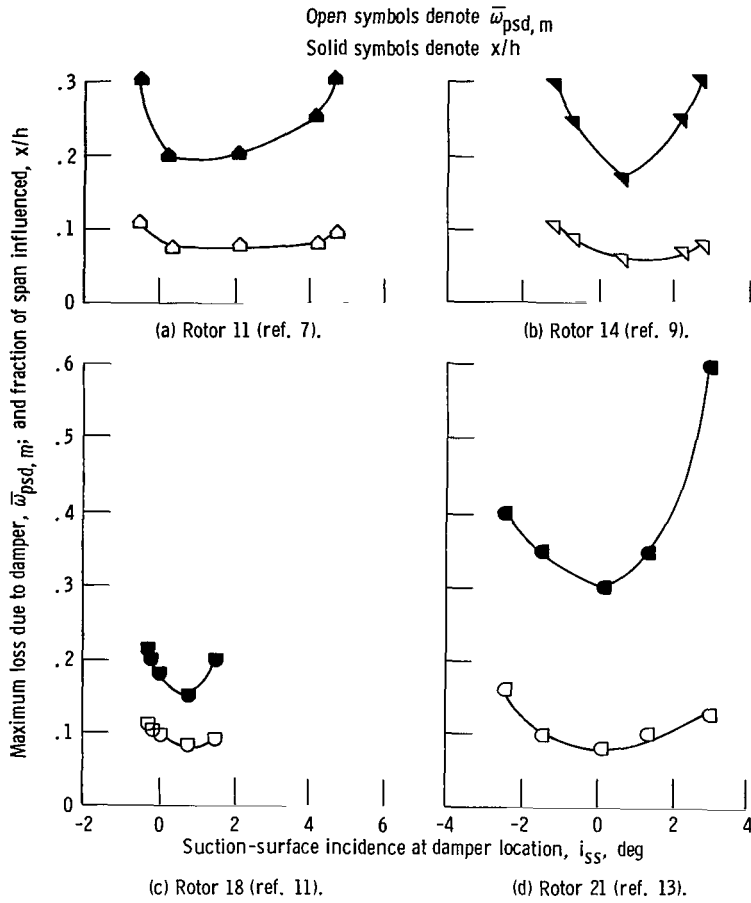


Figure 8. - Performance of part-span damper as function of blade suction-surface incidence at damper location for four NASA rotors.

where the asterisk denotes the minimum and/or reference value; that is,  $\kappa_{psd,m}^*$  and  $(x/h)^*$  are minimum and reference values but  $i_{ss}^*$  is only a reference value at minimum loss and in the region of influence. The differences in loss  $\Delta\bar{\omega}_{psd,m}$  and region of influence  $\Delta(x/h)$  were divided by the aerodynamic loading parameter  $\varphi/\sigma$  before correlation with  $\Delta i_{ss}$  since a highly loaded rotor will tend to show off-design rotor performance deterioration before one that is lightly loaded. Furthermore the data were also correlated with shock loss  $\bar{\omega}_s$  as well as with the loading parameter  $\varphi/\sigma$ . No significant difference was found between this correlation and that shown in figure 9, the data scatter and variation for both relations being virtually the same. Relations of the form

$$\frac{\Delta\bar{\omega}_{psd,m}}{\varphi/\sigma} = 0.02(\Delta i_{ss})^2 \quad (7)$$

and

$$\frac{\Delta(x/h)}{\varphi/\sigma} = 0.06(\Delta i_{ss})^2 \quad (8)$$

correlate most of the data within or near the tolerance band and follow the limits of the data reasonably well. Therefore, if relationships could be developed to give  $i_{ss}^*$ ,  $\bar{\omega}_{psd,m}^*$ , and  $(x/h)^*$  over a range of speeds, damper performance could be estimated for any normal operating condition. (Normal operating condition here is taken to mean speeds between 50 and 100 percent of design.) A plot of the variation with rotor speed of

(1) The difference in blade suction-surface incidence at minimum part-span-damper loss

$$\Delta i_{ss}^* = i_{ss}^* - (i_{ss}^*)_{100}$$

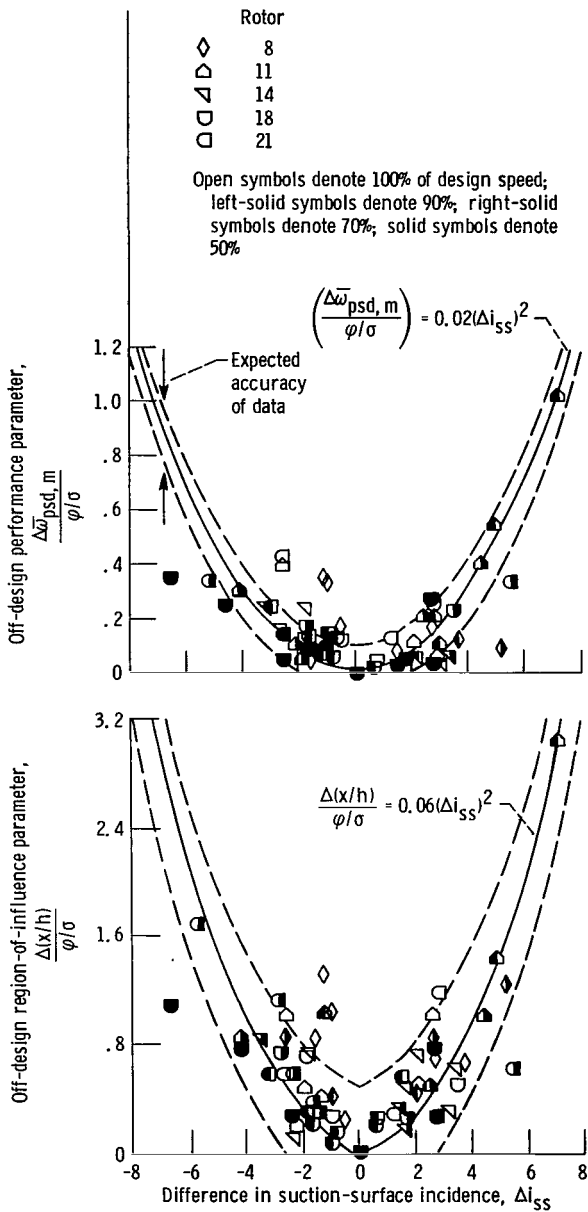


Figure 9. - Off-design performance of part-span damper as function of difference in blade suction-surface incidence at design location for five NASA rotors. (See table I for rotor details.)

(2) The difference in minimum part-span-damper loss coefficient

$$\Delta\bar{\omega}_{psd, m}^* = \bar{\omega}_{psd, m}^* - (\bar{\omega}_{psd, m})_{100}^*$$

(3) The difference in minimum region of influence

$$\Delta\left(\frac{x}{h}\right)^* = \left(\frac{x}{h}\right)^* - \left(\frac{x}{h}\right)_{100}^*$$

is shown in figure 10 for the NASA rotors of table I. Subscript 100 denotes the minimum value at 100 percent of design speed, which according reference 1 correlates well with the design point.

Figure 10 shows that there is a general increase of minimum-loss blade suction-surface incidence with a decrease of rotational speed below design. It was observed from the data that a constant-throttle (or area) operating line through the design point falls

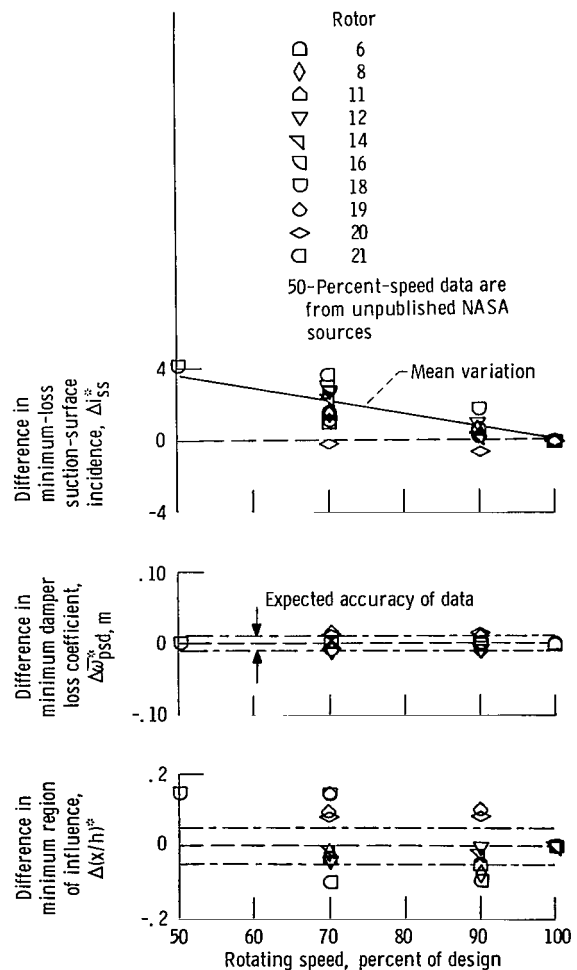


Figure 10. - Differences in minimum-loss blade suction-surface incidence, minimum part-span-damper loss coefficient, and minimum region of influence as function of speed for 10 NASA transonic rotors. (See table I for rotor details.)

near the midrange point of most rotors at any speed between 100 and 50 percent of design. (See appendix B for a discussion of operating line.) Furthermore the point at which the loss due to the damper is a minimum also occurs near the midrange point for most rotors. Therefore, if the blade suction-surface incidence at minimum loss  $i_{ss}^*$  for any operating speed is the same or near that associated with an operating line through the design point, it would be possible to estimate the variation of  $i_{ss}^*$  with rotor speed. Consequently  $i_{ss}^*$  for the 10 NASA rotors of table I was correlated with the blade suction-surface incidence at the damper location predicted by the intersection of a constant-area operating line with 100, 90, 70, and 50 percent speed lines for those rotors. The results are plotted in figure 11 and indicate that, with the exception of three points (out of 31), all the data correlate within the expected accuracy (which is given by NASA for angle measurements as  $\pm 1^\circ$ , refs. 5 to 13 and 17 to 21). Therefore the blade suction-surface incidence, at the damper location, that exists at the intersection of a constant-area operating line through the design point and any normal speed line should serve as a reasonable estimate of minimum-damper-loss, blade suction-surface incidence  $i_{ss}^*$ .

Figure 10 indicates that the minimum-loss coefficient and region of influence are relatively constant between 100 and 50 percent of design speed (although there is significant scatter in the region-of-influence data):

$$\left. \begin{aligned} \bar{\omega}_{psd,m}^* &\approx \text{Constant} \\ \left(\frac{x}{h}\right)^* &\approx \text{Constant} \end{aligned} \right\} \quad (9)$$

It would be expected that the minimum-loss coefficient would decrease with rotational speed since shock losses associated with the damper (fig. 3) will diminish greatly as speed drops off. However, the minimum-loss coefficient and region of influence remain approximately the same as speed decreases, as is shown in figure 10. The most likely explanation for this behavior is variation of the damper angle of attack. As discussed in reference 1, for the NASA rotors the part-span damper was placed along a design streamline, and therefore at design point the damper angle of attack can be expected to be at or very near zero. As the speed is decreased the pressure and density ratios across the rotor fall below design and cause a mismatch between the annulus area and the flow. This results in a streamline shift that changes damper angle of attack from its minimum-loss value. This change is reflected by the increase of

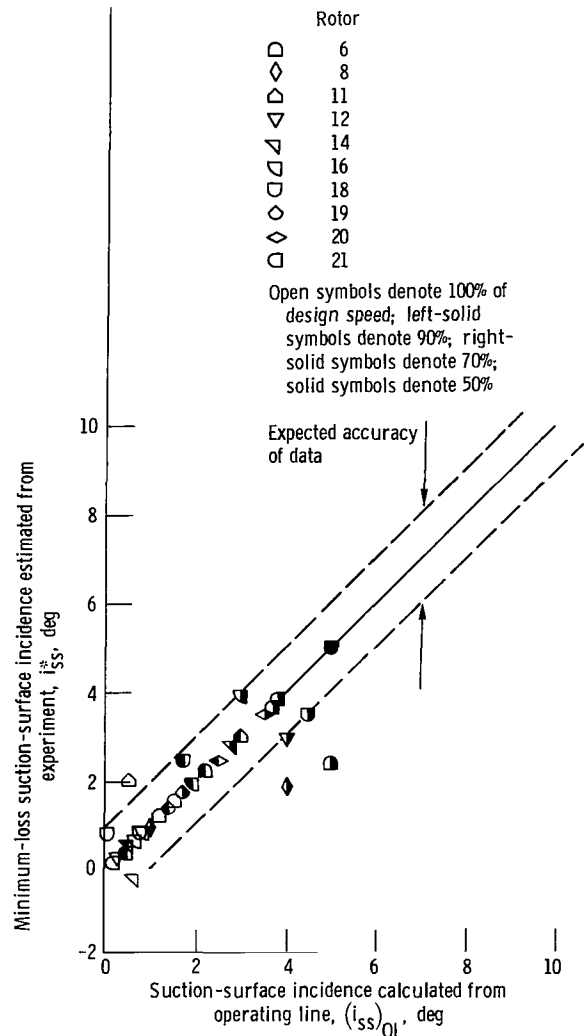
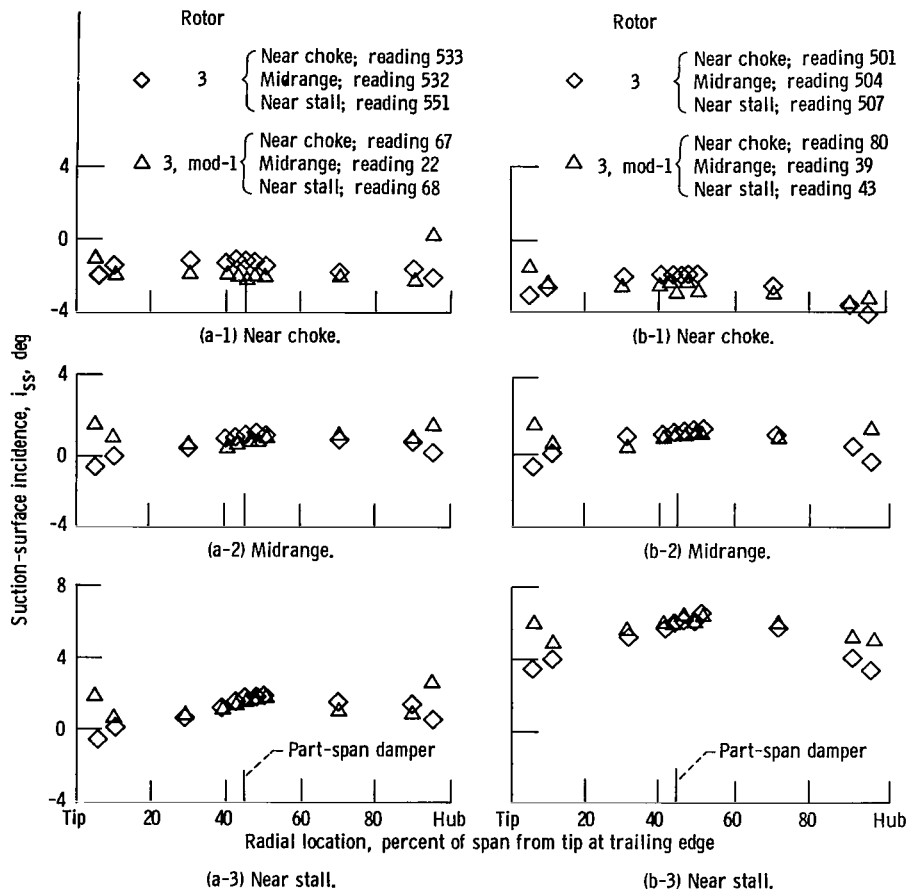


Figure 11. - Correlation of blade suction-surface incidence at damper location calculated from operating line with minimum-damper-loss blade suction-surface incidence at damper location estimated from experiment for 10 NASA transonic rotors. (See table I for rotor details.)

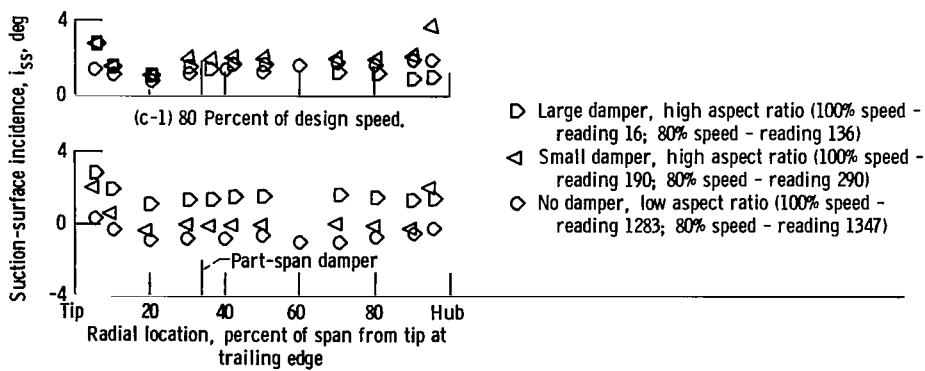
minimum-loss, blade suction-surface incidence. Changing the damper angle of attack will increase the part-span-damper reference loss coefficient  $\bar{\omega}_{psd,m}^*$  and the region of influence  $(x/h)^*$ . The data of figure 10 indicate that, for the rotors used in this correlation, the increase in damper profile loss approximately balances the decrease in shock loss as rotor speed is lowered.

The proposed correlation uses blade suction-surface incidence at the damper location as the off-design geometric loading parameter. This parameter



(a) Rotor 3 (large dampers) and rotor 3, mod-1 (small dampers) for various operating conditions at 100 percent of design speed.

(b) Rotor 3 (large dampers) and rotor 3, mod-1 (small dampers) for various operating conditions at 70 percent of design speed.



(c) Rotor 1 of NASA two-stage fan with large, small, and no part-span dampers operating near maximum efficiency.

Figure 12. - Radial variation of blade suction-surface incidence for different NASA rotors and rotational speeds. (See table I for rotor details.)

will have to be calculated in the absence of experimental data (i.e., for the design and analysis of a new rotor). Therefore it is important to determine the effect that the presence and size of the dampers have on the blade suction-surface incidence in the vicinity of the damper. A plot of blade suction-surface incidence with spanwise location is shown in figure 12 for the same rotors and operating points as in figures 5 and 6. The variation of incidence for variously sized dampers is shown to be small, with the greatest change occurring for the first rotor of the two-stage fan (fig. 12(c)) at 100 percent of design speed. This difference can be attributed in part to the decreased mass flow at design speed for the large damper rotor (ref. 19).

### Application of Correlation

The correlation presented in figures 9 to 12 can be used to estimate the off-design losses of part-span dampers during the analysis of transonic rotors. Once a rotor with a damper has been designed, an off-design code computes a rotor performance map for a constant damper loss and region of influence, which are estimated from the design-point damper correlation (ref. 1). Then a constant-area operating line is calculated, and the blade suction-surface incidence at minimum loss  $i_{ss}^*$  is estimated. After this, an estimate can be made of damper off-design loss for each point of a new rotor performance map. This process is repeated until convergence within an acceptable tolerance occurs.

Equations (1) to (9) can be used with an off-design computer code to predict rotor performance with the following procedure:

(1) Estimate the design-point loss coefficient and region of influence by using equations (1) and (2).

(2) Compute a rotor performance map by using a constant damper loss, found in step 1.

(3) Determine  $i_{ss}^*$  from an operating line—speed line intersection.

(4) Determine  $\bar{\omega}_{psd,m}^*$  and  $(x/h)^*$  from equations (9).

(5) Choose an off-design speed and mass flow and determine  $i_{ss}$  at that point.

(6) Use  $\Delta i_{ss}$  from equation (4) to calculate  $\Delta \bar{\omega}_{psd,m}$  and  $\Delta(x/h)$  from equations (7) and (8). Then the solution of equations (5) and (6) gives an estimate of  $\bar{\omega}_{psd,m}$  and  $x/h$  at the off-design point.

(7) Estimate the spanwise distribution of loss coefficient from the point of maximum damper loss by using equation (3).

(8) Repeat steps (2) to (7) until rotor off-design performance converges within an acceptable tolerance.

The correlation represented by equations (1) to (9) was used to estimate the off-design, part-span-damper performance for one NASA rotor and for the three rotors from NASA-sponsored industrial research given in table I (which were not used to make up the correlation). NASA rotor 6 was chosen for comparison, as figure 11 shows that the  $i_{ss}^*$  at 70 percent of design speed is the furthest from correlation with that given by the operating line—speed line intersection. The correlation was applied to the 70 percent speed line of NASA rotor 6; the results are shown in figure 13. The agreement between correlation and experiment is reasonably

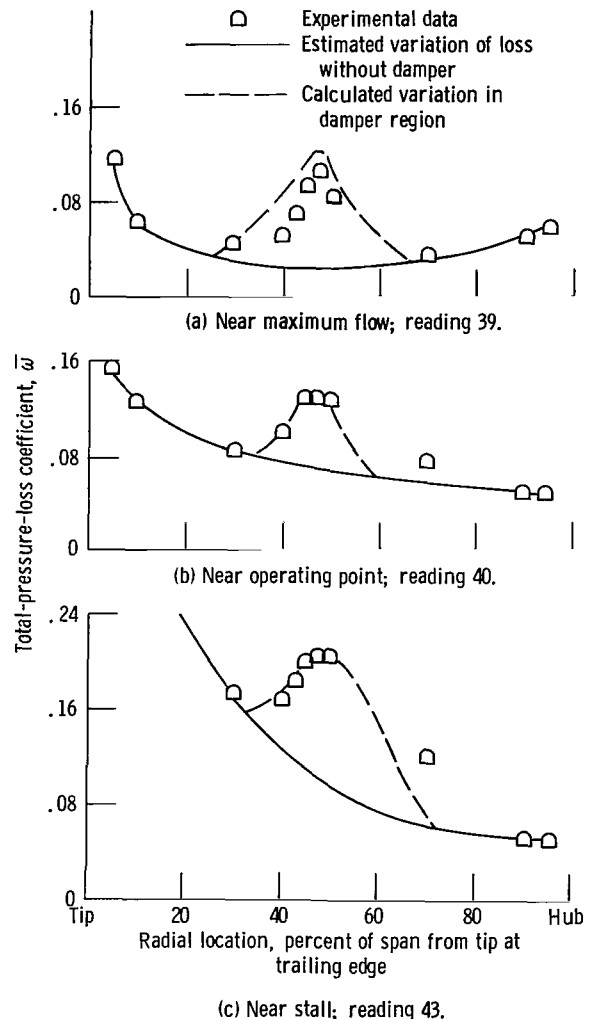


Figure 13. - Comparison between experimental and calculated variation of rotor loss coefficient in region influenced by part-span damper for NASA rotor 6 at various operating conditions at 70 percent of design speed.

good and leads one to expect that the remainder of the NASA rotors would give good agreement.

Figures 14 to 16 compare the radial variation of loss predicted by the correlation with that measured by experiment for the AiResearch, General Electric, and Pratt & Whitney research fans, respectively. The comparison was made for 100, 70, and 50 percent of design speed except for the AiResearch fan, which was not tested at 50 percent speed. Three points on

each speed line (near maximum flow, near the operating point, and near stall) were used for comparison. (The "near operating point" was that data point that occurred nearest to the intersection of the operating and speed lines.) In most instances the agreement was fair to good—except for the Pratt & Whitney rotor at part speed (fig. 16(b)). For this rotor at 70 percent speed the agreement went from fair near maximum flow to poor near stall. A reason

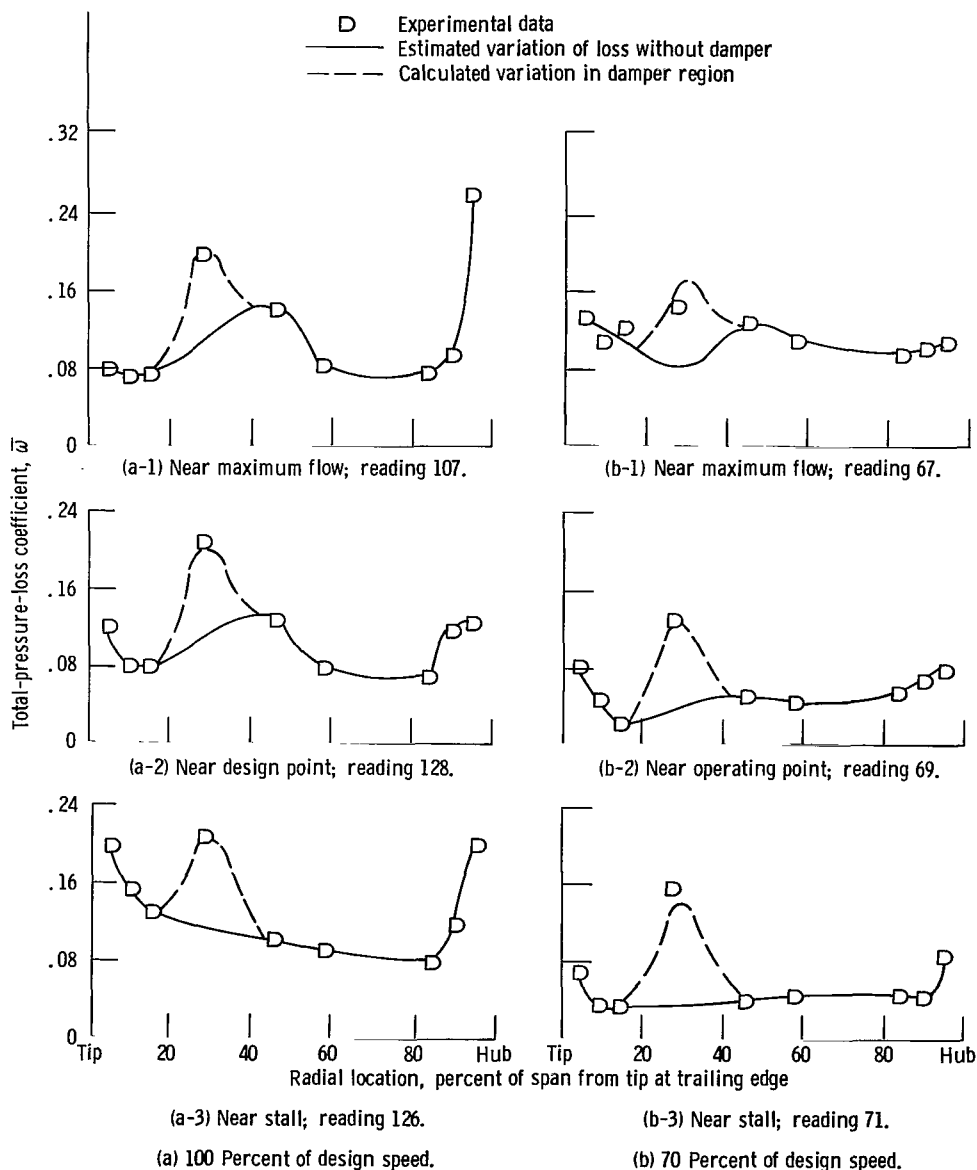


Figure 14. - Comparison between experimental and calculated variation of rotor loss coefficient in region influenced by part-span damper for AiResearch single-stage fan at various operating conditions at two rotating speeds.

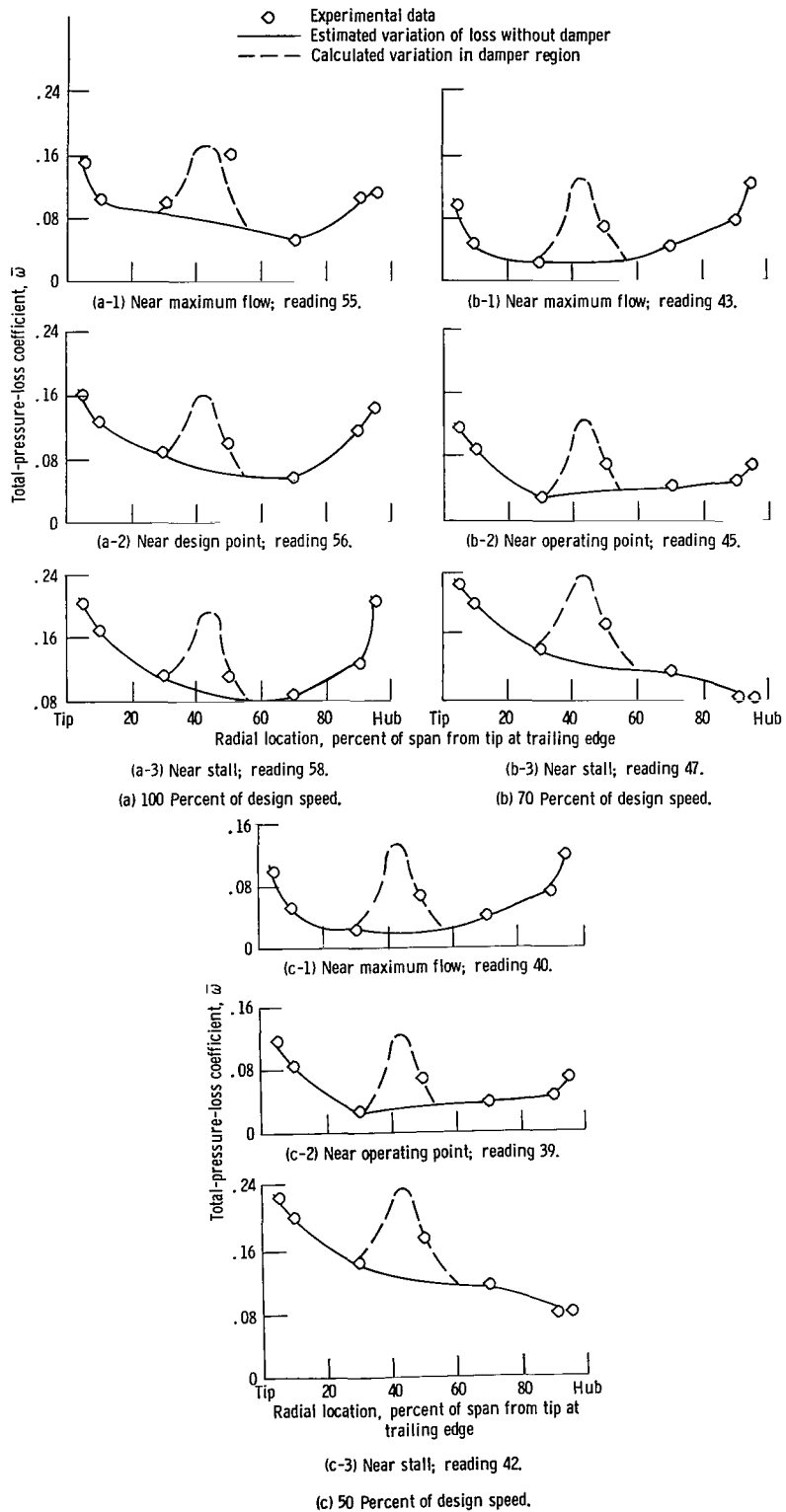


Figure 15. - Comparison between experimental and calculated variation of rotor loss coefficient in region influenced by part-span damper for General Electric Task I rotor at various operating conditions at three rotating speeds.

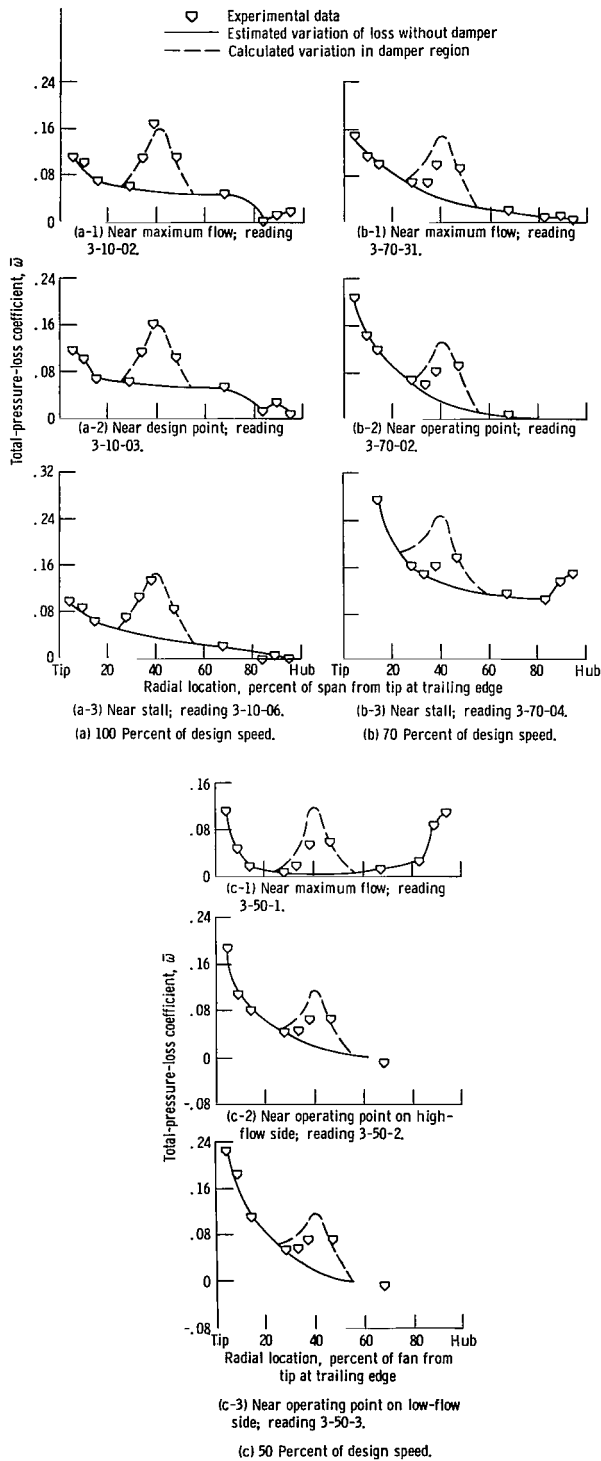


Figure 16. - Comparison between experimental and calculated variation of rotor loss coefficient in region influenced by part-span damper for Pratt & Whitney two-stage fan, rotor 1, at various operating conditions at three rotating speeds.

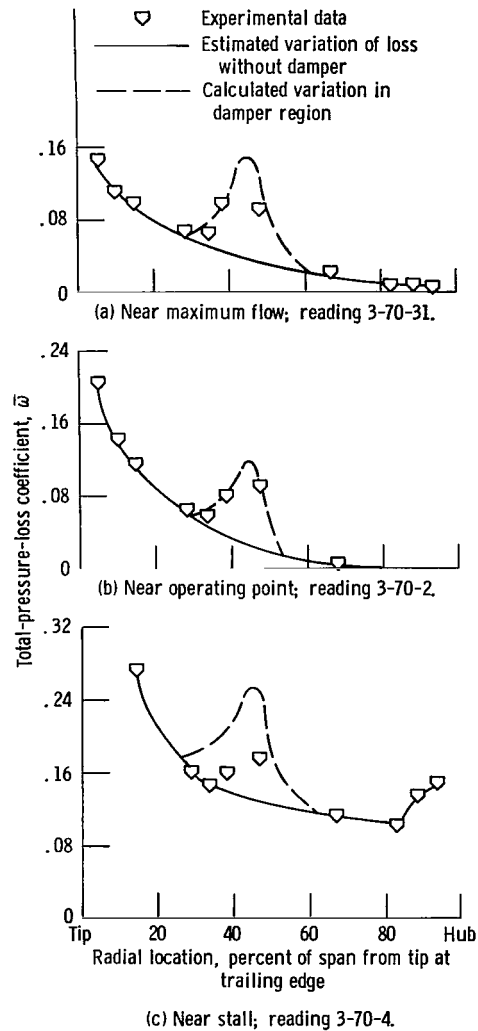


Figure 17. - Comparison between experimental and calculated variation of rotor loss coefficient in region influenced by part-span damper for Pratt & Whitney two-stage fan, rotor 1, at various operating conditions at 70 percent of design speed with maximum damper loss shifted 5 percent of span toward hub.

for this could be the manner in which the data were taken. The radial variation of rotor loss for the General Electric and Pratt & Whitney fans was deduced from traverse and rake data taken behind the stator. Therefore there could be some radial shift of streamlines. In figure 17 the Pratt & Whitney 70-percent-speed-line data have been replotted with the calculated loss region shifted 5 percent of the span toward the hub. With this shift, the near-maximum-flow and operating-point data agreed very well with the prediction. However, the near-stall

point continues to show poor agreement. If, for this near-stall point, the experimental value of the maximum-loss coefficient in the damper region is estimated at 0.20 and the region of influence is estimated at 0.27, the correlation overpredicts by 0.05 and 0.1, respectively. This can serve as an indication of the maximum error expected from the correlation.

## Discussion

As reference 2 indicates, a good estimate of the loss variation in the vicinity of the damper makes it possible to accurately calculate blade row performance over the span. Since the aerodynamic and mechanical forces as well as the blade geometry must be calculated before the required damper size is known, the correlation for damper loss must be used on an iterative basis. Iteration procedures for design (indirect) or analysis (direct) methods can be calibrated by using experimental data from rotors with dampers, so long as the data through the damper region are well defined. Furthermore a correlation of this type could be used to aid in the data reduction for fan stages where measurement directly behind the rotor is not possible, because of blade spacing, as was the case for the General Electric and Pratt & Whitney data of figures 15 and 16.

The present correlation and that of reference 1 were calibrated with fan data taken when a damper was added to the existing blade configuration; that is, the blade shape and thickness were not changed to take into account the additional blockage caused by the presence of the damper. If the blade shape and thickness were modified at the damper location by some form of "area ruling," it is likely that losses would not be so great as indicated herein. Therefore the present correlation would probably be conservative (or high) on predicted damper loss for those fan blades where damper blockage had been allowed for by area ruling. Along with area ruling the chordwise location of the damper could strongly affect the damper loss and region of influence. If the damper were placed near the blade trailing edge behind the main passage shock, the damper loss and region of influence might be substantially reduced. However, aeroelastic integrity might also be compromised.

Knowledge of the spanwise flow variation behind the damper makes it possible to minimize the impact of the damper and its associated losses on performance. It also allows trade-off studies to be made between high-aspect-ratio rotors with dampers

and lower-aspect-ratio rotors without dampers. Finally an estimate of the extent and depth of the damper wake as it propagates downstream through the stator can be used with an off-design code to estimate the local flow effects and to optimize stator performance.

## Concluding Remarks

A correlation is proposed that calculates the off-design performance of part-span dampers. This method is based on rotor performance where the damper was located near the midchord and the blade shape and thickness were not modified to take into account the increase in blockage due to the damper. The data from 10 NASA transonic, axial-flow research rotors were used to formulate the correlation. These rotors had design tip speeds that varied from 419 to 425 meters per second and design pressure ratios that varied from 1.6 to 2.0. The maximum total-pressure losses attributable to the damper and the region influenced were correlated in the following manner for various operating conditions between 50 and 100 percent of design speed:

1. The maximum loss due to the damper and the region influenced at the design point are calculated by the method presented in reference 1 and these values are used as reference quantities for all off-design calculations.

2. The point of intersection of a constant-throttle (or area) operating line with a speed line defines the reference point where damper loss is a minimum. From this point the blade suction-surface incidence at the damper location is determined from experimental data or an off-design analysis code.

3. The damper maximum loss  $\bar{\omega}_{psd,m}$  and region of influence  $x/h$  are calculated for any point on the speed line by taking the difference in the blade suction-surface incidence  $i_{ss}$  at that point and the reference incidence  $i_{ss}^*$  and using it in the following equations:

$$\bar{\omega}_{psd,m} = \bar{\omega}_{psd,m}^* + 0.02 \left( \frac{\varphi}{\sigma} \right) (\Delta i_{ss})^2$$

$$\frac{x}{h} = \left( \frac{x}{h} \right)^* + 0.06 \left( \frac{\varphi}{\sigma} \right) (\Delta i_{ss})^2$$

where  $\Delta i_{ss} = i_{ss} - i_{ss}^*$ , the asterisk indicates minimum and/or reference conditions,  $\varphi$  is camber angle, and  $\sigma$  is solidity.

This correlation was used to predict the off-design damper performance of three NASA-sponsored industrial research rotors that were not used to formulate the correlation. These rotors varied in tip speed, loading, and damper geometry and placement. Comparison with experimental results showed fair to good agreement for most of the data examined.

The correlation should be useful in the design and analysis of axial-flow fan and compressor rotors that use part-span dampers for structural integrity. It allows the local total-pressure-loss variation in the

region of the damper to be estimated for arbitrary operating conditions between 50 and 100 percent of design speed. Using this variation allows the local and overall effects of the damper on the spanwise distribution of pressure, temperature, velocity, efficiency, and flow angle to be computed.

Lewis Research Center,  
National Aeronautics and Space Administration,  
Cleveland, Ohio, February 4, 1980,  
505-04.

# Appendix A

## Symbols

|   |   |
|---|---|
| <p><math>A</math> area, cm<sup>2</sup></p> <p><math>a</math> speed of sound, m/sec</p> <p><math>C_D</math> drag coefficient</p> <p><math>c_d</math> part-span-damper chord, cm</p> <p><math>c</math> blade chord, cm</p> <p><math>d</math> distance between spanwise location of <math>\bar{\omega}_{psd,m}</math> and end of damper region of influence, either toward hub or tip, cm</p> <p><math>h</math> mean blade span, cm</p> <p><math>i_{ss}</math> incidence angle to blade suction surface, angle between inlet air direction and line tangent to blade suction surface at leading edge, deg</p> <p><math>K_1, K_2</math> constants</p> <p><math>M</math> Mach number</p> <p><math>\bar{M}</math> mean inlet Mach number, average of inlet Mach number ahead of blade and maximum suction-surface Mach number calculated by method of ref. 4</p> <p><math>P</math> total pressure, N/cm<sup>2</sup></p> <p><math>p</math> static pressure, N/cm<sup>2</sup></p> <p><math>R</math> specific gas constant, 287.05 J/kg K</p> <p><math>r</math> spanwise radius in meridional plane, cm</p> <p><math>r_{le}</math> leading-edge, part-span-damper radius, cm</p> <p><math>r_{te}</math> trailing-edge, part-span-damper radius, cm</p> <p><math>T</math> temperature, K</p> <p><math>t</math> part-span-damper maximum thickness, cm</p> <p><math>W</math> mass flow, kg/sec</p> <p><math>W(\sqrt{\theta}/\delta)</math> equivalent mass flow, kg/sec</p> <p><math>x</math> part-span-damper spanwise region of influence, cm</p> <p><math>\alpha</math> angle of attack, deg</p> <p><math>\gamma</math> ratio of specific heats</p> | <p><math>\delta</math> pressure correction factor, <math>P/P_{ref}</math></p> <p><math>\eta</math> stage adiabatic efficiency</p> <p><math>\theta</math> temperature correction factor, <math>T/T_{ref}</math></p> <p><math>\rho</math> density, kg/cm<sup>3</sup></p> <p><math>\sigma</math> solidity, ratio of blade chord to spacing</p> <p><math>\varphi</math> camber angle, rad</p> <p><math>\bar{\omega}</math> total-pressure-loss coefficient, <math>[(P_2)_{id} - P_2]/(P_1 - p_1)</math></p> <p><math>\bar{\omega}_p</math> profile loss coefficient, <math>\bar{\omega} - \bar{\omega}_s</math></p> <p><math>\bar{\omega}_s</math> shock loss coefficient, <math>\bar{\omega} - \bar{\omega}_p</math></p> <p>Subscripts:</p> <p><math>d</math> damper</p> <p><math>dr</math> damper region</p> <p><math>dr,m</math> maximum loss in damper region</p> <p><math>h</math> hub</p> <p><math>id</math> ideal</p> <p><math>m</math> location of maximum damper loss</p> <p><math>max</math> maximum</p> <p><math>o</math> estimated loss level in absence of a part-span-damper</p> <p><math>psd,m</math> maximum additional loss due to part-span-damper (fig. 4)</p> <p><math>ref</math> NASA standard conditions (<math>P_{ref} = 10.133</math> N/cm<sup>2</sup>, <math>T_{ref} = 288.2</math> K)</p> <p><math>s</math> normal shock</p> <p><math>t</math> tip</p> <p>0 ambient conditions</p> <p>1 stage inlet</p> <p>2 stage outlet</p> <p>3 nozzle exit plane</p> <p>100 100 percent of design speed</p> <p>Superscripts:</p> <p>*</p> <p>minimum loss and/or reference conditions relative to blade row</p> |
|---|---|

## Appendix B

### Operating Line

A constant-throttle (or area) operating line is determined by the outlet area a fan "sees" downstream. This is illustrated in figure 18. A fan stage is moved along a fixed speed line by "throttling" the flow, that is, changing the outlet or nozzle area to increase or decrease the mass flow through the machine. An operating line is determined by fixing the throttle setting or nozzle area of a fan and varying the rotational speed. If the operating point falls within the fan's operating range for that speed, the pressure ratio will adjust itself to the outlet area until choking occurs. Any point of a fan-pressure-ratio-corrected mass flow performance map can be used to define an operating line by finding all operating points that fall on a constant-area line through that point. An operating line might run through a reference such as the design point, the maximum-efficiency point, or a point with a specified stall margin. Once the reference point through which the operating line must pass is chosen, a nozzle area must be found that corresponds to this reference point. If expansion to ambient pressure is used to size the nozzle and the pressure loss between the fan outlet and the nozzle outlet is assumed to be zero,

$$\text{Nozzle area} = A_3 = \frac{W}{\rho_3 V_3} = \frac{W}{\rho_3 a_3 M_3} \quad (\text{B1})$$

$$A_3 = \frac{W}{\rho_2 (\rho_3 / \rho_2) a_2 (a_3 / a_2) M_3} \quad (\text{B2})$$

Now  $\rho = P/RT$  and  $a = \sqrt{\gamma RT}$ .

Substituting these relations into equation (B2) and rearranging terms give

$$A_3 = K \left[ \frac{W(\sqrt{\theta/\delta})}{(P_2/P_1 / \sqrt{T_2/T_1})(\rho_3/\rho_2)(a_3/a_2)M_3} \right] \quad (\text{B3})$$

where

$$\frac{T_2}{T_1} = 1 + \frac{1}{\eta} \left[ \left( \frac{P_2}{P_1} \right)^{(\gamma-1)/\gamma} - 1 \right]$$

and  $K$  is a constant that depends on the gas and the system of units used,

$$K = \left[ \frac{\sqrt{T_{ref}/P_{ref}}}{\sqrt{\gamma/R}} \right]$$

and  $W(\sqrt{\theta/\delta})$  is the equivalent weight flow (symbols defined in appendix A). Pressure loss between the fan and the nozzle outlet can be taken into account by multiplying the pressure ratio  $P_2/P_1$  by a loss factor.

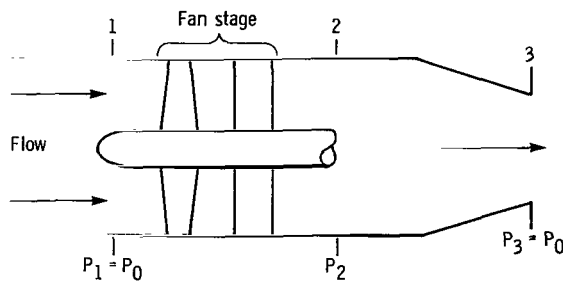


Figure 18. - Schematic of fan nozzle.

The operating line used in this report is one that passes through the design point. From the design pressure ratio, mass flow, and efficiency a nozzle area is calculated for a zero pressure loss between the fan and the nozzle outlet. After the nozzle area is found, the operating line is determined by finding the operating points on several speed lines that have performance that matches the design-point nozzle area; that is, the area calculated by using equation (B3) is equal to the design-point nozzle area. Constant-area operating lines were determined for all the rotors used to make up figure 11 and those rotors used to verify the correlation. An example of a constant-area operating line through the design point is given in figure 19 for NASA rotor 6. The nozzle areas from the data points available seldom exactly match those necessary to be on the operating line. However, if sufficient data are taken along a speed line, one data point will be close. In some instances the operating line passes between two points, and the intersection of the operating and speed lines must be interpolated.

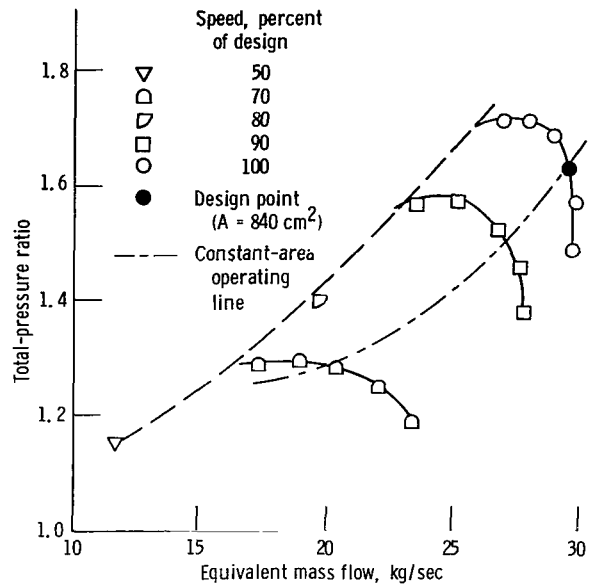


Figure 19. - Overall performance for stage 6-1 (ref. 10).

## References

1. Roberts, William B.: Correlation of Part-Span Damper Losses Through Transonic Rotors Operating Near Design Point. NASA TM X-3542, 1977. (Also ASME Paper 78-GT-153, Apr. 1978.)
2. Esgar, Genevieve M.; and Sandercock, Donald M.: Some Observed Effects of Part-Span Dampers on Rotating Blade Row Performance Near Design Point. NASA TM X-2696, 1973.
3. Benser, W.A.; Bailey, E.E.; and Gelder, T.F.: Holographic Studies of Shock Waves Within Transonic Fan Rotors. Power, vol. 97, no. 1, Jan. 1975, pp. 75-84.
4. Schwenk, Francis C.; Lewis, George W.; and Hartmann, Melvin J.: A Preliminary Analysis of the Magnitude of Shock Losses in Transonic Compressors. NACA RM E57A30, 1957.
5. Kovich, George; and Reid, Lonnie: Overall and Blade-Element Performance of a Multiple-Circular-Arc Bladed Transonic Compressor Rotor with Tip Speed of 1375 Feet per Second. NASA TM X-2697, 1973.
6. Osborn, Walter M.; Urasek, Donald C.; and Moore, Royce D.: Performance of a Single-Stage Transonic Compressor with a Blade-Tip Solidity of 1.5 and Comparison with 1.3- and 1.7-Solidity Stages. NASA TM X-2926, 1973.
7. Kovich, George; Moore, Royce D.; and Urasek, Donald C.: Performance of a Transonic Fan Stage with Weight Flow per Unit Annulus Area of 198 Kilograms per Second per Square Meter (40.6(lb/sec)/ft<sup>2</sup>). NASA TM X-2905, 1973.
8. Moore, Royce D.; and Reid, Lonnie: Performance of a Single-Stage Axial-Flow Transonic Compressor Stage with a Blade Tip Solidity of 1.7. NASA TM X-2658, 1972.
9. Urasek, Donald C.; Moore, Royce D.; and Osborn, Walter M.: Performance of a Single-Stage Transonic Compressor with a Blade Tip Solidity of 1.3. NASA TM X-2645, 1972.
10. Moore, Royce D.; Urasek, Donald C.; and Kovich, George: Performance of Transonic Fan Stage with Weight Flow per Unit Annulus Area of 178 Kilograms per Second per Square Meter (36.5 (lb/sec)/ft<sup>2</sup>). NASA TM X-2904, 1973.
11. Lewis, George W., Jr.; Reid, Lonnie; and Tysl, Edward R.: Design and Performance of a High-Pressure-Ratio, Highly Loaded Axial-Flow Transonic Compressor Stage. NASA TM X-3100, 1974.
12. Moore, Royce D.; Lewis, George W., Jr.; and Osborn, Walter M.: Performance of a Transonic Fan Stage Designed for Meridional Velocity Ratio of 0.8. NASA TP-1298, 1978.
13. Schmidt, James F.; and Ruggeri, Robert S.: Performance With and Without Inlet Radial Distortion of a Transonic Fan Stage Designed for Reduced Loading in the Tip Region. NASA TP-1294, 1978.
14. Ware, T.C.; Kobayashi, R.F.; and Jackson, R.J.: High-Tip-Speed, Low-Loading Transonic Fan Stage. Part 3, Final Report (AIRESEARCH-73-9488-Pt3, AiResearch Mfg. Co., NASA Contract NAS3-13498.) NASA CR-121263, 1974.
15. Koch, C.C.; Bilwakesh, K.R.; and Doyle, V.L.: Evaluation of Range and Distortion Tolerance for High Mach Number Transonic Fan Stages. Vol. 1, Final Report. (GE-R71-AEG-133-VOL-1, General Electric Co.; NASA Contract NAS3-11157.) NASA CR-72806, 1971.
16. Messenger, H.E.; and Keenan, M.J.: Two-Stage Fan. 2: Data and Performance with Redesigned Second-Stage-Rotor Uniform and Distorted Inlet Flows. (PWA-5087, Pratt & Whitney Aircraft, NASA Contract NAS3-13494.) NASA CR-134710, 1974.
17. Hager, Roy D.; Janetske, David C.; and Reid, Lonnie: Performance of a 1380 Foot per Second Tip Speed Axial-Flow Compressor Rotor with a Blade Tip Solidity of 1.3. NASA TM X-2448, 1972.
18. Lewis, George W., Jr.; and Urasek, Donald C.: Comparison of the Effect of Two Damper Sizes on the Performance of a Low-Solidity Axial-Flow Transonic Compressor Rotor. NASA TM X-2536, 1972.
19. Urasek, Donald C.; Cunnann, Walter S.; and Stevens, William: Performance of Two-Stage Fan with Large Dampers on First-Stage Rotor. NASA TP-1399, 1979.
20. Cunnann, Walter S.; Stevens, William; and Urasek, Donald C.: Design and Performance of 427-Meter-per-Second-Tip-Speed Two-Stage Fan Having a 2.40 Pressure Ratio. NASA TP-1314, 1978.
21. Urasek, Donald C.; Gorrell, William T.; and Cunnann, Walter S.: Performance of Two-Stage Fan Having Low-Aspect-Ratio First-Stage Blading. NASA TP-1493, 1980.

|  |  |  |  |
|--|--|--|--|
| 1. Report No.<br>NASA TP-1693  | 2. Government Accession No.                          | 3. Recipient's Catalog No.   |  |
| 4. Title and Subtitle<br>OFF-DESIGN CORRELATION FOR LOSSES DUE TO<br>PART-SPAN DAMPERS ON TRANSONIC ROTORS   |  | 5. Report Date<br>July 1980  | 6. Performing Organization Code                          |
|  |  | 8. Performing Organization Report No.<br>E-309   | 10. Work Unit No.<br>505-04                              |
| 7. Author(s)<br>William B. Roberts, James E. Crouse,<br>and Donald M. Sandercock   |  | 11. Contract or Grant No.  | 13. Type of Report and Period Covered<br>Technical Paper |
| 9. Performing Organization Name and Address<br>National Aeronautics and Space Administration<br>Lewis Research Center<br>Cleveland, Ohio 44135   |  | 14. Sponsoring Agency Code   |  |
|  |  | 12. Sponsoring Agency Name and Address<br>National Aeronautics and Space Administration<br>Washington, D. C. 20546 |  |
| 15. Supplementary Notes<br>William B. Roberts, formerly with University of Notre Dame; James E. Crouse and<br>Donald M. Sandercock, Lewis Research Center.   |  |  |  |
| 16. Abstract<br><br>The experimental data from 10 transonic fan rotors were used to correlate losses created by part-span dampers located near the midchord position on the rotor blades. The design tip speed of these rotors varied from 419 to 425 m/sec, and the design pressure ratio varied from 1.6 to 2.0. The additional loss caused by the dampers for operating conditions between 50 and 100 percent of design speed were correlated with relevant aerodynamic and geometric parameters. The resulting correlation predicts the variation of total-pressure-loss coefficient in the damper region to a good approximation. |  |  |  |
| 17. Key Words (Suggested by Author(s))<br>Part-span dampers<br>Compressor losses   |  | 18. Distribution Statement<br>Unclassified - unlimited<br>STAR Category 07   |  |
| 19. Security Classif. (of this report)<br>Unclassified   | 20. Security Classif. (of this page)<br>Unclassified | 21. No. of Pages<br>23   | 22. Price*<br>A02  |

\* For sale by the National Technical Information Service, Springfield, Virginia 22161

NASA-Langley, 1980

National Aeronautics and  
Space Administration

THIRD-CLASS BULK RATE

Postage and Fees Paid  
National Aeronautics and  
Space Administration  
NASA-451



Washington, D.C.  
20546

Official Business

Penalty for Private Use, \$300

3 1 1U,A, 071180 S00903DS  
DEPT OF THE AIR FORCE  
AF WEAPONS LABORATORY  
ATTN: TECHNICAL LIBRARY (SUL)  
KIRTLAND AFB NM 87117

**NASA**

POSTMASTER: If Undeliverable (Section 158  
Postal Manual) Do Not Return

---